From: LIGHT SCATTERING BY IRREGULARY SHAPED PARTICLES
Edited by Donald W. Schuerman
(Plenum Publishing Corporation, 1980)

LIGHT SCATTERING BY HEXAGONAL COLUMNS AND PLATES

Kuo-Nan Liou and Rich F. Coleman

University of Utah, Department of Meteorology

Salt Lake City, Utah 84112

ABSTRACT

Computations of light scattering by hexagonal columns and plates randomly oriented in two- and three-dimensional space are carried out by means of the geometrical ray tracing technique. Analyses are made for a number of crystal sizes, and for a visible wavelength of 0.55 μm and an infrared wavelength of 10.6 μm at which absorption plays a significant role. Scattering phase functions and degree of linear polarization computed from the ray tracing program are compared with those derived from experimental nephelometer measurements performed in the laboratory. Effects of the crystal size and shape on the scattering parameter will be described. We will also present the theoretical and experimental programs concerning light scattering by ice clouds to be carried out in the future.

1. INTRODUCTION

Cloud compositions change constantly and drastically with respect to time and space depending upon such variables as temperature, saturation ratio and atmospheric conditions. Perhaps there is no unique shape, size and orientation for the irregularly shaped ice crystals in the atmosphere.

Information on the scattering characteristics of non-spherical ice crystals is imperative to the development of remote sensing techniques for the cloud composition determination and to the understanding of the radiation budget of cirrus cloudy atmospheres.

In this paper we present some results of scattering and polarization calculations for hexagonal plates and columns by means of

geometrical ray tracing and present comparisons of these scattering and polarization calculations with measured values obtained from the laboratory laser scattering and cloud physics experiments.

2. RAY TRACING FOR HEXAGONAL CRYSTALS

The general geometry of light rays incident on a hexagonal crystal is depicted in Figure 1. The geometry of the crystal is defined by the length L and radius R, while the incident light rays are described by the ray plane. Normal to the Z-axis, we define the principle plane, which lies on the X-Y plane. A hexagon has six equal sides and the top and bottom faces. To describe the geometry of the hexagon with respect to the incident ray plane, seven variables are required, *i.e.*, the length and radius of the hexagon and the position of the principal plane, the position of the incident ray on the ray axis, and three angles defining the orientation of the crystal with respect to the incident ray, *i.e.*, the elevation angle θ, the rotation angle Ψ and the azimuthal angle ϕ.

Having defined the variables involved, the ray tracing procedures may be outlined. We first find the position of the entry ray in the (X,Y,Z) coordinates in terms of the seven geometrical variables. Through Snell's law, we find the refracted angles in terms of the incident angle mapped on the principal plane and the elevation angle. It follows that the position of the exit ray, the face that the ray will hit and the geometrical path length in the crystal can be determined through the procedures of the analytical geometry. The procedures are then repeated for internally reflected rays. Finally, we need to find the scattering angle with respect to the incident ray, to perform the summation of the refracted and reflected components and to carry out the normalization of the energy pattern to get the scattering phase function.

The geometrical ray tracing equations for hexagons differ greatly from those for spheres. Spheres have a curvature effect, whereas hexagons do not. Also, a hexagon does not have the symmetry of the geometrical path length that a sphere inherently possesses. Basically, the general equation for the scattered energy per unit angle normalized with respect to the incident energy perpendicular to the X-Z plane may be described by

$$E^s_{\ell,r}(\Theta,P) = \sum_j E^s_{\ell,r}(\Theta,P,\tau_j)\, e^{-2km_i\ell_p} \sum_j \cos\tau_{1j} \qquad (1)$$

(equation (1) continues)

$$= \frac{e^{-2km_i\ell_p}}{\Sigma \cos\tau_{1j}} \begin{cases} \Sigma\, |r_{\ell,r}(\tau_{1j})|^2 \cos\tau_{1j}, & P=0 \text{ (external reflection)} \\ \Sigma\, [1-|r_{\ell,r}(\tau_{1j})|^2][1-|r_{\ell,r}(\tau_{2j})|^2] \cos\tau_{1j}, & P=1 \text{ (two refraction)} \\ \Sigma\, [1-|r_{\ell,r}(\tau_{1j})|^2][1-|r_{\ell,r}(\tau_{(P-1)j})|^2] \times \prod_{n=2}^{P} |r_{\ell,r}(\tau_{nj})|^2 \cos\tau_{1j}, & P\geq 2 \text{ (internal reflection)} \end{cases}$$

where subscripts ℓ and r denote the parallel and perpendicular polarization components, respectively, Θ the scattering angle, j the index for the entry rays, ℓ_p the ray path length in the crystal ($\ell_p=0$, when P=0), τ_1 the incident angle, which normally has three different values, p the index denoting the event of reflection and refraction and τ_2, τ_3,... are incident angles in the crystal. Since absorption is considered, absolute values need to be taken for the reflection and transmission components. Scattering energy patterns for two-dimensional and three-dimensional orientations may be subsequently computed by noting the specific relation of the incident angle and the elevation and azimuthal angles. For horizontal orientation cases, the incident angle is the elevation angle. But for general cases $\cos\tau = \cos\theta \cos\phi$.

The Snell's law governing the incident angles (θ,ϕ) and refracted angles (θ',ϕ') can be proven to be

$$\begin{aligned} m_r \sin\theta' &= \sin\theta \\ m_r \frac{\cos\theta'}{\cos\theta} \sin\phi' &= \sin\phi \end{aligned} \qquad (2)$$

where m_r is the real index of refraction.

To complete the ray tracing exercise, we have to include the diffraction pattern. The projection of a hexagonal column onto a horizontal plane clearly resembles a rectangle. The diffraction pattern for a rectangular aperture can be easily derived from Franhofer diffraction theory. It is given by

$$E^d(\Theta,\phi,L) = \frac{\sin^2(Rk \sin\Theta \cos\phi)}{(Rk \sin\Theta \cos\phi)^2} \frac{\sin^2[(Lk/2) \sin\Theta \sin\phi)}{[(Lk/2) \sin\Theta \sin\phi]^2} \qquad (3)$$

where k is the wavenumber and R is the radius of the crystal. Clearly, three parameters are required to define the position of a hexagon in

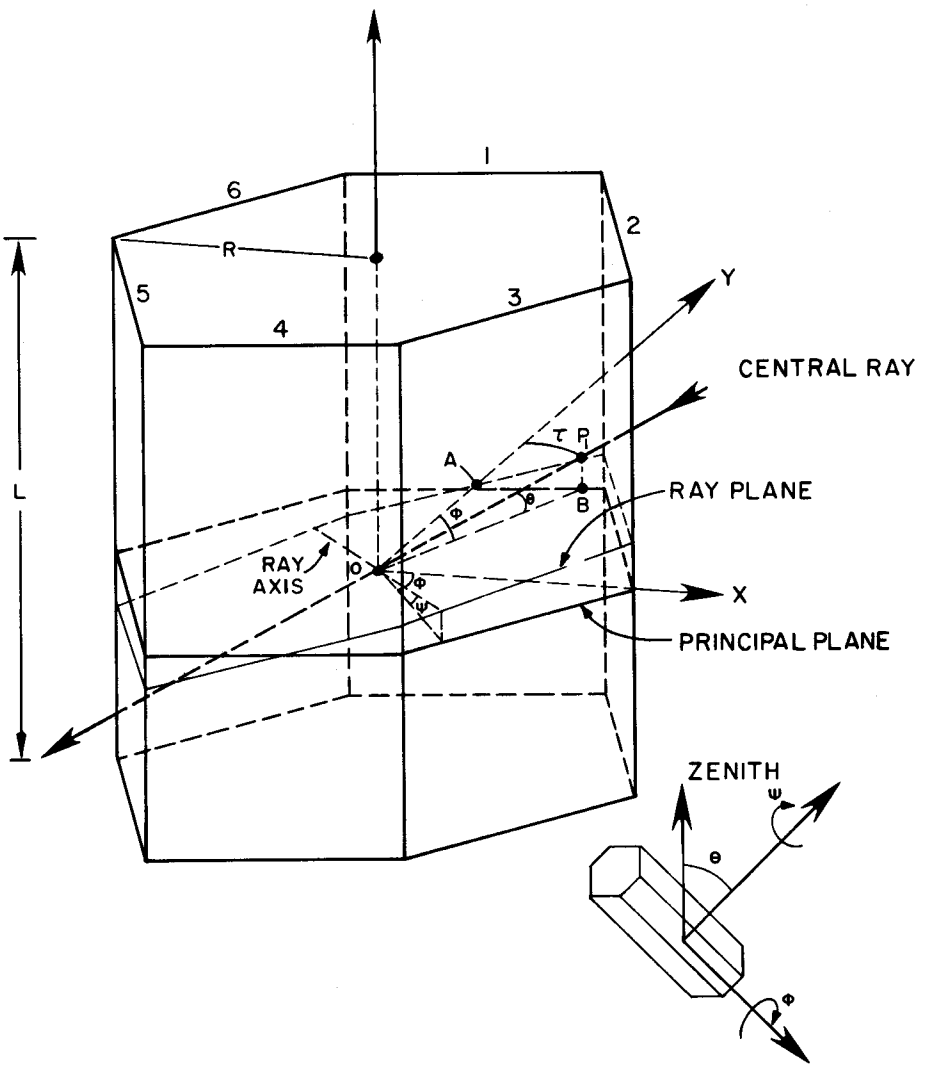

FIG. 1. General geometry of light rays incident on a hexagonal crystal.

reference to the incident ray, *i.e.*, the scattering angle Θ, the azimuthal angle ϕ and the geometrical length L. For horizontally oriented hexagons the diffraction pattern can be obtained by performing integration in ϕ from 0 to π, *i.e.*,

$$E^d_{2D}(\Theta,L) = \frac{1}{\pi}\int_0^{\pi} E^d(\Theta,\phi,L)\, d\phi \quad . \tag{4}$$

For three-dimensional random orientation, integration with respect to the length of hexagons is required. Thus, we find

$$E^d_{3D}(\Theta) = \begin{cases} \dfrac{1}{(1/2-R)}\displaystyle\int_R^{L/2} E^d_{2D}(\Theta,L')\, dL' , & \text{columns} \\ \dfrac{1}{(R-L/2)}\displaystyle\int_{L/2}^{R} E^d_{2D}(\Theta,L')\, dL' , & \text{plates} . \end{cases} \tag{5}$$

It should be noted that for plates, the approximate equation is less accurate because the major axis is on the plane of the hexagon.

Since the equations derived from the ray tracing procedure are in units of energy per degree, we must perform a normalization so that the scattering phase function can be derived. On the basis of the definition of gain with respect to isotropic scatterers, we find

$$\frac{G(\Theta)\ 2\pi\ \sin\Theta\ d\Theta\ r^2}{4\pi r^2} = E(\Theta)\, d\Theta \tag{6}$$

where r denotes the distance and the gain is normalized such that

$$\frac{1}{4\pi}\int_{4\pi} G(\Theta)\ \sin\Theta\ d\Theta d\phi = 1 \ . \tag{7}$$

Thus, the gain is equivalent to the phase function commonly used in radiative transfer.

3. RESULTS AND DISCUSSIONS

Figure 2 shows the scattering patterns due to geometrical reflection and refraction for horizontally oriented and randomly oriented columns with lengths and radii of 300 and 60 μm, respectively, incident by a visible wavelength of 0.55 μm. The index P in the

diagram denotes the contribution of the scattering energy; P=0, external reflection, P=1, two refractions, and P $\geq$ 2, internal reflection. The dashed and dashed-dot lines represent the scattering patterns for horizontally oriented columns with elevation angles of 0° (normal incidence) and 42°, respectively, while the solid curve denotes the scattering pattern for random orientation. The major features for these three cases are the strong forward scattering and halo in the region of 20°-30°. For horizontal orientation, the halo feature shifts to a larger scattering angle when the incident angle increases. We see a 8° difference for incident angles of 0° and 42°. Owing to the shift of the halo features for different incident angles, the halo feature in the case of random orientation is broadened and smeared out. The less pronounced 46° halo features are also evident in cases of random orientation and horizontal orientation with normal incidence. The strong peak at 84° in the case of horizontal orientation with an incident angle of 42° is strictly due to the external reflection. Note that the scattering pattern beyond 84° is caused by the end effects and internal reflections. For random orientation and horizontal orientation with normal incidence, the backscattering is primarily produced by one internal reflection. The less pronounced backscattering in random orientation case is the result of the averaging over many oblique incidence cases.

Shown in Figure 3 are the normalized scattering phase functions, which include both the diffraction and geometrical reflection and refraction contributions, for horizontally oriented plates with parallel incidence for two wavelengths of 0.55 and 10.6 μm. (The random orientation pattern for plates will be discussed in the next paragraph.) At the wavelength of 10.6 μm, the real and imaginary parts of the refractive index are, respectively, 1.097 and 0.134. Clearly, absorption must be significant. Comparison with a real refractive index of 1.31 for the 0.55 μm wavelength shows that from about 50 to 180° the scattering is much reduced, especially in the backscattering directions where one internal reflection, which is the dominant contributor to the scattering process, is decreased due to significant absorption. At the 10.6 μm wavelength, plates also produce a halo feature at 7° but its magnitude is on the same order as the forward diffraction value. Thus, it does not become differentiable from the forward diffraction peak. The diffraction peak for 10.6 μm is much broadened and its maximum intensity is much smaller than that for 0.55 μm as shown in Figure 3.

Comparison of the scattering phase functions for randomly oriented columns with lengths of 300 μm and radii of 60 μm and plates with radii of 125 μm and lengths 25 μm is illustrated in Figure 4. The most significant scattering differences between plates and columns are the much lower forward peak for plates and the much lower side scattering for columns. The 22° and the less pronounced 46° halos for columns are relatively stronger than those for plates. Both scattering patterns depict the very narrow diffraction peak, strong

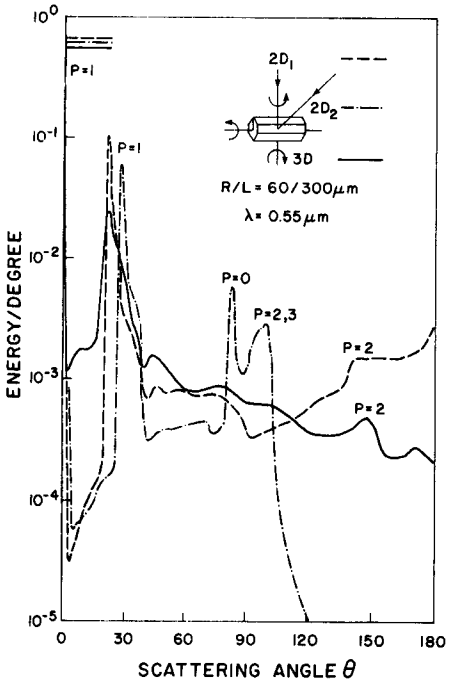

FIG. 2. Scattered energy per degree for randomly oriented columns (3D) and for horizontally oriented columns (2D) with elevation angles θ of 0° and 42°.

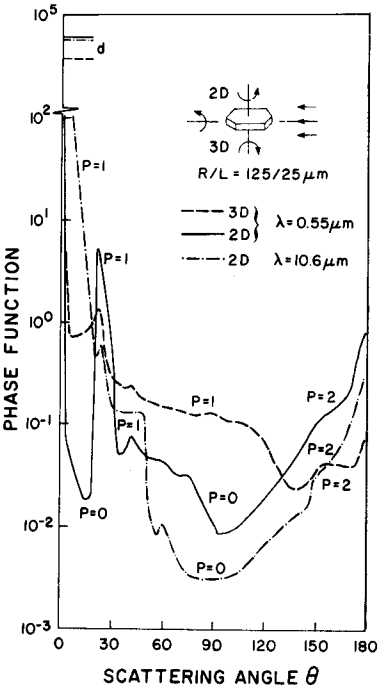

FIG. 3. Phase functions for randomly oriented plates (3D) and for horizontally oriented plates (2D) with elevation angles θ of 0° and 42°.

22° halo feature and broad peak at about 150°. The shift in the 150° peak from columns to plates appear to be due to the fact that randomly oriented columns are much more like a spheroid than plates.

The degree of linear polarization is shown in Figure 5 for randomly oriented columns and plates as well as for spheres based on the geometrical ray tracing for comparison purposes. The polarization pattern for plates remains negative from 0° to about 66°, whereas for columns negative polarization only extends from 0° to about 39°. The strong polarization maximum for plates at about 136° is caused by external reflection (p = 0). Such a maximum occurs at about 70° for columns. The positive polarization peaks at about 156° and 178° for columns associated with one internal reflection (p = 2). There is a slight negative polarization for plates in the backscattering direction from about 165° to 180°. The polarization patterns for non-spherical plates and columns differ significantly from the polarization produced by spheres. Large spheres (*i.e.*, in

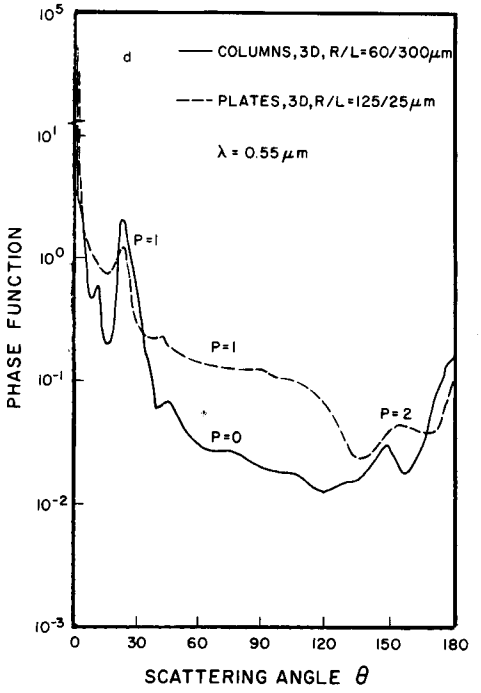

FIG. 4. Phase functions for randomly oriented (3D) columns and plates.

geometrical regions) generate strong polarization at about 80° due to the external reflection and at the first (~138°) and second (~126°) rainbow angles caused by one and two internal reflections, respectively. The apparent and significant differences in polarization patterns caused by the shape factor may provide a practical and feasible means for the identification of spheres, plate-like and column-like particles in clouds. Also shown in this figure is the polarization pattern derived from experimental data for plates having a modal diameter of 20 μm. There is general agreement between the measured and calculated polarization patterns for plates despite the size difference.

Figure 6 shows comparisons of the normalized phase functions for plates derived from a number of nephelomemeter measurements in the laboratory (Sassen and Liou, 1979) and from ray tracing calculations. Three samples of plates with modal diameters of 1.5, 3.5 and 20 μm were produced in the cold chamber during the scattering experiments. Experimental values reveal that the side scattering for plates increases when the particle size increases. This increase is contrary to the scattering behavior of spherical water drops whose side scattering in the normalized scattering phase function generally reduces with increasing sizes. The much larger side scattering from ray optics calculations is physically understandable in view of the large plates considered. Figure 7 illustrates another comparison of the normalized phase function for clouds composed of a mixture of small plates and columns obtained from three scattering measurements with that derived from ray tracing calculations for columns. Again, the ray optics results show much stronger side scattering and a pronounced 22° halo as well as a less noted 46° halo, which small columns and plates are unable to produce. Note that the forward scattering for small columns and plates is greater than that of large columns in the regions from about 10° to 20°.

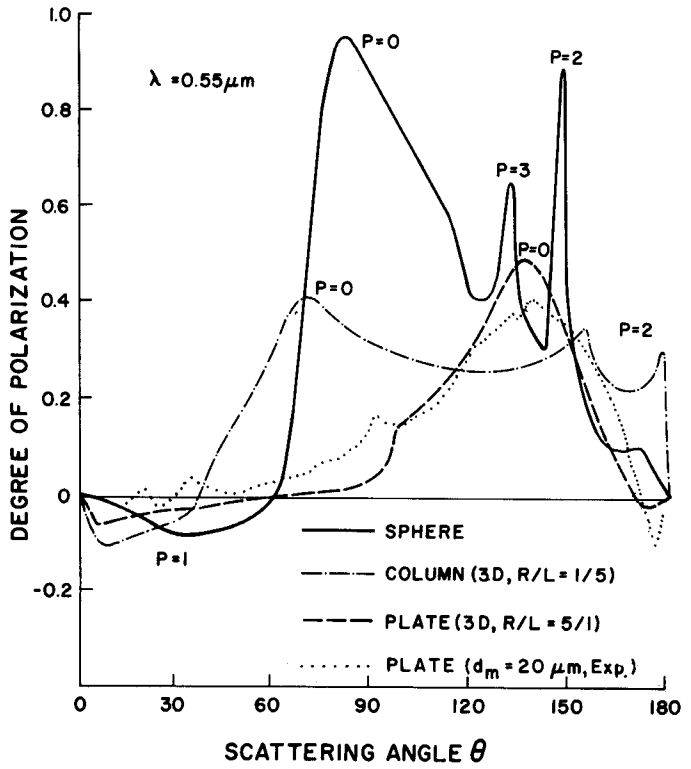

FIG. 5. The degree of linear polarization for randomly oriented columns and plates and for spheres. Also shown is the polarization pattern derived from experimental data for plates having a modal diameter of 20 μm.

It would be desirable to generate larger plates and columns in the cloud chamber so that more significant comparisons between measured scattering data and ray optics calculations could be carried out to cross-check the experimental and theoretical results more

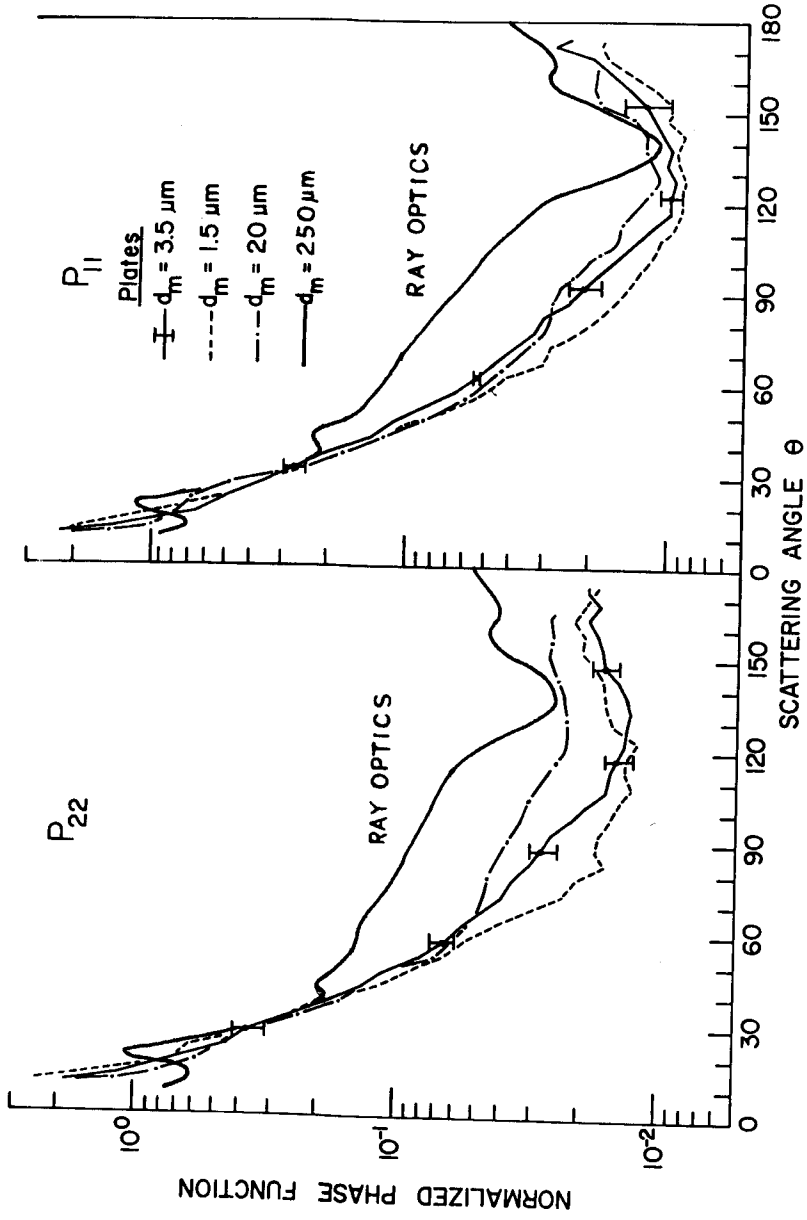

FIG. 6. Normalized phase function for plates from a number of nephelometer measurements in the laboratory and from ray tracing calculations.

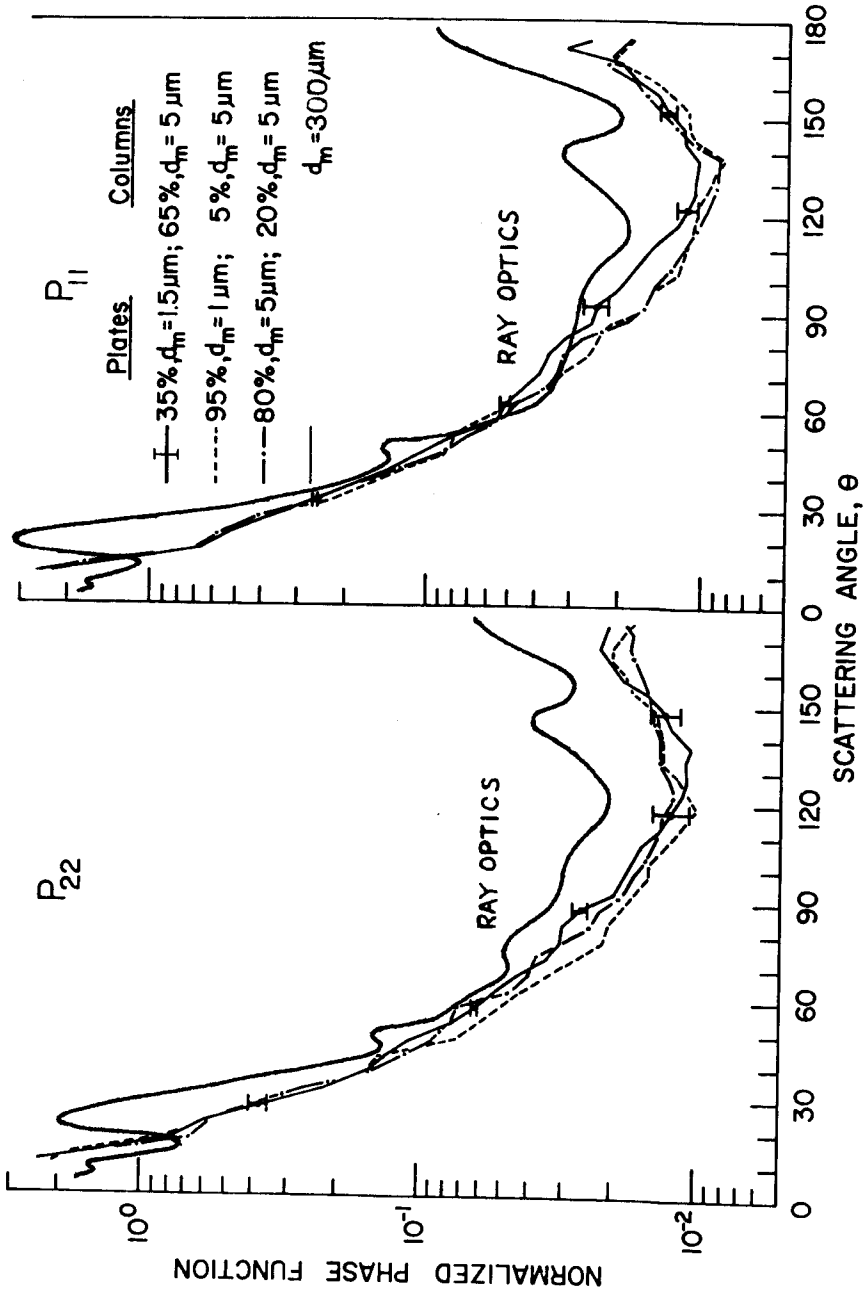

FIG. 7. Normalized phase function for mixtures of plates and columns from a number of nephelometer measurements in the laboratory and for columns from ray tracing calculations.

reliably and comprehensively. Finally, it should be noted that information and physical understanding of the basic scattering parameters for oriented columns and plates are required to perform radiative transfer calculations for cirrus clouds and to develop active remote sensing techniques for the identification of the phase, shape and size of cloud particles.

Acknowledgements. This research was supported by the Meteorology Program, Division of Atmospheric Sciences, National Science Foundation under Grant ATM78-26259.

Questions (JAYAWEERA): In natural clouds, the basic shapes you described are more the exception than the rule. To what extent could you apply the ray tracing technique to derive the scattered intensities from natural ice crystals? Also, would it be more prudent to look to an empirical relation for scattering functions of natural ice crystals because the ray tracing for these crystals will be extremely time consuming and laborious?

Answer (LIOU): In answer to your questions, I would like to point out that the fact that we see halo phenomena in the atmosphere indicates that a large number of ice crystals have basic hexagonal column and plate structures. To understand physically the scattering characteristics of ice crystals, it is necessary, but not sufficient, to perform theoretical analyses and computations in terms of the ray tracing technique. As you have correctly pointed out, naturally occurring ice crystals have in general more complex shapes than these simple columns and plates. It is, therefore, extremely important to carry out controlled laboratory light scattering experiments in which known sizes and shapes and perhaps orientations may be generated and to make use of the experimental results to assess the theoretical computations. I have shown in my presentation some comparisons between results derived from ray tracing computations and laboratory scattering measurements. Moreover, I also feel that it is significant to conduct field scattering experiments involving ice crystals so that quantitative scattering properties of natural ice crystals can be obtained under a variety of atmospheric conditions. However, without theoretical analyses and computations, it is not possible to understand the physical significance of particular scattering features and general properties of irregularly shaped ice crystals in conjunction with remote sensing exploration and radiative transfer studies.

REFERENCE

Sassen, K. and Liou, K. N., 1979, *J. Atmos. Sci.*, *36*, 838-851.